The Estimation of Temperature Distribution in Cylindrical Battery Cells Under Unknown Cooling Conditions

Youngki Kim, *Member, IEEE*, Shankar Mohan, *Student Member, IEEE*, Jason B. Siegel, *Member, IEEE*, Anna G. Stefanopoulou, *Fellow, IEEE*, and Yi Ding

***Abstract*— The estimation of temperature inside a battery cell requires accurate information about the cooling conditions even when the battery surface temperature is measured. This paper presents a model-based approach for estimating temperature distribution inside a cylindrical battery under unknown convective cooling conditions. A reduced-order thermal model using a polynomial approximation of the temperature profile inside the battery is used. A dual Kalman filter (DKF), a combination of a Kalman filter and an extended Kalman filter, is then applied for the identification of the convection coefficient and the estimation of the battery core temperature. The thermal properties are modeled by volume averaged lumped-values under the assumption of a homogeneous and isotropic volume. The model is parameterized and validated using experimental data from a 2.3 Ah 26 650 lithium-iron-phosphate battery cell with a forced-air convective cooling during hybrid electric vehicle drive cycles. Experimental results show that the proposed DKF-based estimation method can provide an accurate prediction of the core temperature under unknown cooling conditions by measuring battery current and voltage along with surface and ambient temperatures.**

***Index Terms*— Dual Kalman filter (DKF), lithium ion (Li-ion) batteries, reduced-order model, state and parameter estimation, thermal modeling.**

I. Introduction

OVER the past few decades, energy storage systems utilizing lithium ion (Li-ion) batteries have become one of the most critical components for realizing efficient and clean transportation systems through electrification of vehicles, e.g., hybrid electric vehicles (HEVs), plug-in HEVs, and EVs. Li-ion batteries have several advantages such as minimal memory effect, broad temperature range of operation, and high power discharge capability [1], [2]. However, cycle life and capacity of the Li-ion battery are adversely affected by sustained operation at high temperatures [3]–[6]. This presents a problem in automotive applications where high discharge and charge rates needed for vehicle propulsion and regenerative braking cause internal heating of the battery. Knowledge of the temperature distribution across cells and packs in addition to cooling condition allows one to accurately estimate power capability accounting for thermal limits [7]. Thus, being able to estimate/predict is vital for formulating power management and cooling strategies to maximize battery utilization in a supervisory controller.

The battery temperature distribution depends on the convection coefficient, which in turn is influenced by the flow rate of the cooling system. This flow rate can be actively controlled by variable speed motors and pumps. This flexibility requires several experiments to parameterize the convection coefficient. However, the performance of the cooling system can degrade generally due to various reasons such as dust on fan blades, partial blockage in pipes, motor/pump ageing, and even a motor/pump failure. Even though such a degradation or failure can be detected by a fault detection system via pressure and temperature sensors, the battery management system still needs to identify the convection coefficient even in these conditions for an accurate estimation of the core temperature.

This paper considers a novel method for estimating the temperature distribution inside cylindrical batteries with simultaneous estimation of the convective cooling condition. To achieve this goal, the computationally efficient thermal model for a cylindrical battery proposed in [8] is used. A polynomial approximation (PA) to the solution of the heat transfer problem is used as a model reduction technique unlike existing reduced-order modeling approaches in [9]–[13]. This modeling approach facilitates a systematic prediction of the core, the surface and the volume-averaged temperatures along with the volume-averaged temperature gradient. A dual Kalman filter (DKF) is then applied for the identification of the convection coefficient and the temperature distribution inside a cylindrical battery based on measured signals such as the battery current and voltage along with battery surface and ambient temperatures [14]. The proposed method can be augmented with other existing battery thermal or power management strategies in [7] and [15] for the safe and robust operation.

Manuscript received April 29, 2013; revised November 1, 2013; accepted February 5, 2014. Manuscript received in final form February 28, 2014. This work was supported in part by the Automotive Research Center through the Cooperative Agreement under Grant W56HZV-04-2-0001 and in part by the U.S. Army Tank Automotive Research, Development and Engineering Center, Warren, MI, USA. Recommended by Associate Editor S. Varigonda.

Y. Kim, J. B. Siegel, and A. G. Stefanopoulou are with the Department of Mechanical Engineering, University of Michigan, Ann Arbor, MI 48109 USA (e-mail: youngki@umich.edu; siegeljb@umich.edu; annastef@umich.edu).

S. Mohan is with the Department of Electrical Engineering, University of Michigan, Ann Arbor, MI 48109 USA (e-mail: elemsn@umich.edu).

Y. Ding is with the U.S. Army Tank Automotive Research, Development, and Engineering Center, Warren, MI 48397 USA (e-mail: yi.ding8.civ@mail.mil).

Color versions of one or more of the figures in this paper are available online at http://ieeexplore.ieee.org.

Digital Object Identifier 10.1109/TCST.2014.2309492

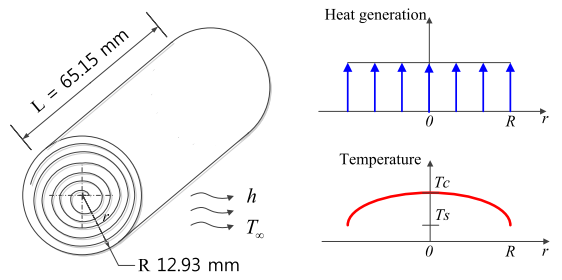

(a) (b)

Fig. 1. (a) Schematic for a A123 26650 cylindrical battery and (b) parabolic temperature profile under uniform heat generation.

This paper is organized as follows. Section II presents the convective heat transfer problem for a cylindrical battery and the reduced-order thermal model. Model reduction is performed applying a PA of the solution of a partial differential equation (PDE) system. The thermal properties of the battery are experimentally identified and the sensitivity of temperature prediction to changes in model parameters is numerically analyzed in Section III. In Section IV, the adaptive temperature estimator is developed applying a DKF for estimating the core temperature and identifying the convection coefficient. Section V presents and discusses the experimental results, and conclusion is drawn in Section VI.

II. Heat Transfer Problem in Cylindrical Batteries

This paper considers the radially distributed (1-D) thermal behavior of a cylindrical battery cell with convective heat transfer boundary condition, as shown in Fig. 1(a) [8], [9], [16], [17]. A cylindrical Li-ion battery, so-called a jelly roll, is fabricated by rolling a stack of cathode/separator/anode layers. The individual layered sheets are thin, therefore, lumped parameters are used so that material properties such as thermal conductivity, density, and specific heat coefficient are assumed to be constant in a homogeneous and isotropic body. For spiral wound current collectors with multiple connections to the battery tab, it is reasonable to assume uniform heat generation along the radial direction [17], [18]. The thermal conductivity is one or two orders of magnitude higher in the axial direction than in the radial direction. Therefore, the temperature distribution in the axial direction will be more uniform [19], [20]. Under these assumptions, the governing equation of the 1-D temperature distribution $T(r,t)$ and boundary conditions are given by

$$\rho c_p \frac{\partial T(r,t)}{\partial t} = k_t \frac{\partial^2 T(r,t)}{\partial r^2} + \frac{k_t}{r}\frac{\partial T(r,t)}{\partial r} + \frac{Q(t)}{V_b} \quad (1)$$

$$\text{B.C.'s } \left.\frac{\partial T(r,t)}{\partial r}\right|_{r=0} = 0 \quad (2)$$

$$\left.\frac{\partial T(r,t)}{\partial r}\right|_{r=R} = -\frac{h}{k_t}(T(R,t) - T_\infty) \quad (3)$$

where ρ, c_p, and k_t represent the volume-averaged density, the specific heat coefficient, and the thermal conductivity of the battery, respectively, and are summarized in Table I. The radius of the battery is R, Q is the heat generation inside the battery, and V_b is the volume of battery. The ambient temperature and the convection coefficient are denoted by T_∞ and h, respectively. The boundary condition in (2) represents the symmetric structure of the battery about the core. The other boundary condition shown in (3) represents the convective heat transfer at the surface of the battery.

TABLE I
Parameters of the Battery [9]

Parameter	Symbol	Value	Unit
Density	ρ	1824	kg/m^3
Specific heat coeff.	c_p	825	J/kgK
Thermal conductivity	k_t	0.488	W/mK
Convection coeff.	h	5	W/m^2-K
Radius	R	12.93e-3	m
Height	L	65.15e-3	m
Volume	V_b	3.4219e-5	m^3

A. Model Reduction

With evenly distributed heat generation, the temperature distribution along r-direction of the battery cell is assumed to satisfy the following PA in [8] [Fig. 1(b)]:

$$T(r,t) = a(t) + b(t)\left(\frac{r}{R}\right)^2 + d(t)\left(\frac{r}{R}\right)^4 \quad (4)$$

where $a(t)$, $b(t)$, and $d(t)$ are the time-varying constants. To satisfy the symmetric boundary condition at the core of the battery cell, (4) contains only even powers of r. Thus, the temperatures at core and surface of the battery can be expressed as

$$T_c = a(t) \quad (5)$$

$$T_s = a(t) + b(t) + d(t) \quad (6)$$

where subscripts c and s denote core and surface, respectively.

The volume-averaged temperature $\bar{T}$ and temperature gradient $\bar{\gamma}$ are introduced as follows:

$$\bar{T} = \frac{2}{R^2}\int_0^R rT dr \quad (7)$$

$$\bar{\gamma} = \frac{2}{R^2}\int_0^R r\left(\frac{\partial T}{\partial r}\right) dr. \quad (8)$$

These volume-averaged values are used as the states unlike existing approaches in [10], [11], and [13].

By substituting (4) in (7) and (8), $\bar{T}$ and $\bar{\gamma}$ can be expressed in terms of time-varying constants as

$$\bar{T} = a(t) + \frac{b(t)}{2} + \frac{d(t)}{3} \quad (9)$$

$$\bar{\gamma} = \frac{4b(t)}{3R} + \frac{8d(t)}{5R}. \quad (10)$$

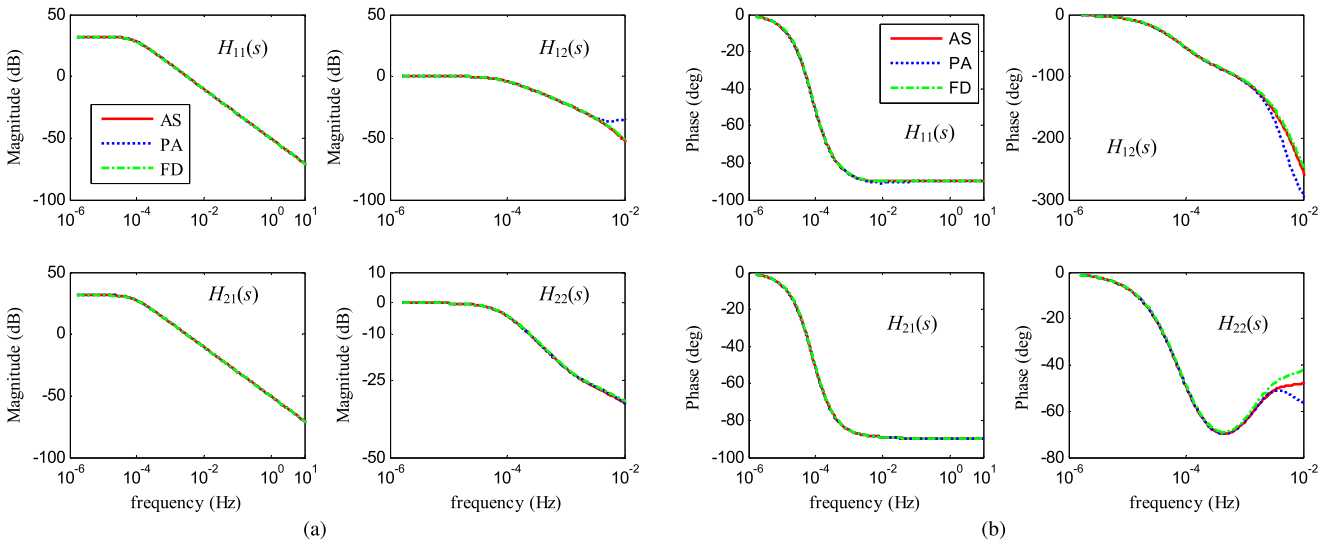

Fig. 2. Comparison of frequency response functions obtained by AS, PA, and FD method. (a) Magnitude. (b) Phase.

By rearranging (6), (9), and (10), time-varying functions $a(t)$, $b(t)$, and $d(t)$ can be written by

$$a(t) = 4T_s - 3\bar{T} - \frac{15R}{8}\bar{\gamma} \tag{11}$$

$$b(t) = -18T_s + 18\bar{T} + \frac{15R}{2}\bar{\gamma} \tag{12}$$

$$d(t) = 15T_s - 15\bar{T} - \frac{45R}{8}\bar{\gamma}. \tag{13}$$

By substituting (11)–(13) in (4), the temperature distribution can be expressed as a function of T_s, $\bar{T}$, and $\bar{\gamma}$

$$\begin{aligned} T(r,t) = {} & 4T_s - 3\bar{T} - \frac{15R}{8}\bar{\gamma} \\ & + \left[-18T_s + 18\bar{T} + \frac{15R}{2}\bar{\gamma}\right]\left(\frac{r}{R}\right)^2 \\ & + \left[15T_s - 15\bar{T} - \frac{45R}{8}\bar{\gamma}\right]\left(\frac{r}{R}\right)^4. \end{aligned} \tag{14}$$

By substituting (14) to following volume-averaged governing equation and its partial derivative with respect to r:

$$\int_0^R \left(\rho c_p \frac{\partial T(r,t)}{\partial t} - k_t \frac{\partial^2 T(r,t)}{\partial r^2} - \frac{k_t}{r}\frac{\partial T(r,t)}{\partial r} - \frac{Q(t)}{V_b}\right) dr = 0$$

$$\int_0^R \frac{\partial}{\partial r}\left(\rho c_p \frac{\partial T(r,t)}{\partial t} - k_t \frac{\partial^2 T(r,t)}{\partial r^2} - \frac{k_t}{r}\frac{\partial T(r,t)}{\partial r} - \frac{Q(t)}{V_b}\right) dr = 0$$

the PDE (1) can be converted into ODEs as follows:

$$\frac{d\bar{T}}{dt} + \frac{48\alpha}{R^2}\bar{T} - \frac{48\alpha}{R^2}T_s + \frac{15\alpha}{R}\bar{\gamma} - \frac{\alpha}{k_t V_b}Q = 0$$

$$\frac{d\bar{\gamma}}{dt} + \frac{320\alpha}{R^3}\bar{T} - \frac{320\alpha}{R^3}T_s + \frac{120\alpha}{R^2}\bar{\gamma} = 0$$

where $\alpha = k_t/\rho c_p$ is thermal diffusivity.

Finally, a two-state thermal model can be given by the following form:

$$\begin{aligned} \dot{x} &= Ax + Bu \\ y &= Cx + Du \end{aligned} \tag{15}$$

where $x = [\bar{T}\ \ \bar{\gamma}]^T$, $u = [Q\ \ T_\infty]^T$, and $y = [T_c\ \ T_s]^T$ are the states, inputs, and outputs, respectively. System matrices A, B, C, and D are defined as follows:

$$A = \begin{bmatrix} \dfrac{-48\alpha h}{R(24k_t + Rh)} & \dfrac{-15\alpha h}{24k_t + Rh} \\ \dfrac{-320\alpha h}{R^2(24k_t + Rh)} & \dfrac{-120\alpha(4k_t + Rh)}{R^2(24k_t + Rh)} \end{bmatrix}$$

$$B = \begin{bmatrix} \dfrac{\alpha}{k_t V_b} & \dfrac{48\alpha h}{R(24k_t + Rh)} \\ 0 & \dfrac{320\alpha h}{R^2(24k_t + Rh)} \end{bmatrix}$$

$$C = \begin{bmatrix} \dfrac{24k_t - 3Rh}{24k_t + Rh} & -\dfrac{120Rk_t + 15R^2h}{8(24k_t + Rh)} \\ \dfrac{24k_t}{24k_t + Rh} & \dfrac{15Rk_t}{48k_t + 2Rh} \end{bmatrix}$$

$$D = \begin{bmatrix} 0 & \dfrac{4Rh}{24k_t + Rh} \\ 0 & \dfrac{Rh}{24k_t + Rh} \end{bmatrix}. \tag{16}$$

This state-space representation is used for the parametrization in Section III and the estimation of core temperature and convection coefficient in Section IV.

B. Frequency Domain Analysis

The transfer function of the thermal system $H(s)$ is calculated by

$$H(s) = D + C(sI - A)^{-1}B$$

where s is Laplace variable and I is the identity matrix.

The frequency response functions of the reduced-order model are compared with those of the analytical solution (AS) in [9] and finite difference (FD) method with 30 discretization. Parameters used to generate the plots in Fig. 2(a) and (b) are summarized in Table I. The heat transfer coefficient of $h = 5$ W/m^{2}K is chosen since this value is typical of natural convection condition [21].

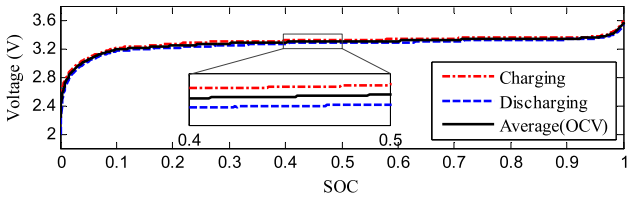

Fig. 3. OCV approximately obtained by averaging terminal voltages during charging and discharging a battery with C/20 current rate.

Fig. 2(a) and (b) show that the effects of heat generation on core and surface temperature, denoted by $H_{11}(s)$ and $H_{21}(s)$, respectively, can be accurately predicted over the whole range of frequency. On the other hand, the responses of core and surface temperature excited by the ambient temperature, $H_{12}(s)$ and $H_{22}(s)$, are nearly identical to the AS for frequencies below 10^{-2} Hz. In general, the temperature of cooling media does not change rapidly. Therefore, the prediction of temperature distribution using the reduced-order model can be considered reasonably accurate.

C. Heat Generation Calculation

Since heat generation rate Q is the input to the battery thermal system, the input needs to be accurately calculated from measurement data, such as current and voltage during operation. Bernardi *et al.* [22] proposed the simplified form of heat generation rate with assumptions that heat generation due to enthalpy-of-mixing, phase-change, and heat capacity are assumed to be negligible as expressed by

$$Q = i(U - V) - i\left(T\frac{\partial U}{\partial T}\right) \tag{17}$$

where i, U, and V represent the current, the open-circuit voltage (OCV), and the terminal voltage, respectively. As shown in Fig. 3, the OCV is a function of the battery state-of-charge (SOC). This function is experimentally obtained by averaging the measured terminal voltages during charging and discharging a battery with C/20 current rate under a constant current constant voltage charging protocol. The OCV is then calculated at the estimated SOC value by integrating measured current with respect to time as

$$\frac{d\text{SOC}}{dt} = -\frac{I}{3600C_b}$$

where C_b is the battery capacity in Ah. The sign convention is such that positive current denotes battery discharging.

The last term in (17) is the heat generation from entropy change. In this paper, heat generation due to entropy change is neglected for simplicity. This simplification is warranted since the typical SOC range of HEV operation is narrow in which $\partial U/\partial T$ of the battery cell is insignificant, as shown in [11] for this chemistry. In addition, the reversible entropic heat generation would have zero mean value when the battery is operating in charge-sustaining mode, typical of HEV operation.

III. Parameter Identification

In this section, the values of lumped parameters for a 2.3 Ah 26650 lithium-iron-phosphate ($LiFePO_4$ or LFP) battery cell by A123 are identified through experimentation using the reduced-order model. Fig. 4 shows current, voltage, and ambient temperature profiles over the urban-assault cycle (UAC) in [23] that is used for the parametrization. This cycle used for simulating military ground vehicles has significantly high power demands. The parameterized model is then validated using measurement data over a different HEV driving cycle. The numerical analysis on parameter sensitivity on temperature prediction is performed to investigate the use of constant parameters for thermal conductivity and heat capacity and the importance of identifying the convection coefficient on-line.

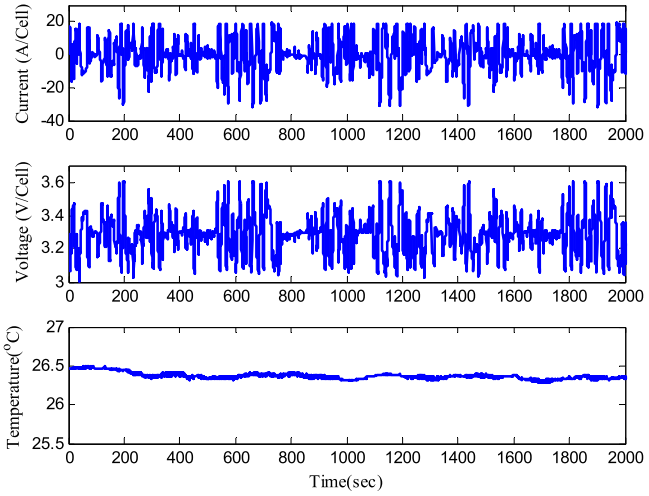

Fig. 4. Data set used for parameter ID: current (top), voltage (middle), and ambient temperature (bottom) during UAC.

A. Identifying Thermal Properties

The parameter identification is important for accurately predicting the temperature distribution inside a battery cell as the parameters k_t, c_p, ρ, and h determine the dynamics of thermal model. As the density is a measurable constant, only three parameters such as k_t, c_p, and h are considered for the parameter identification. The experimental setup for the parameter identification is described in [25]. Measured cell current, voltage, surface and core temperature of the battery cell, and ambient temperature are used for the parameter identification.

Specifically, convection coefficient h is controlled by the fan speed based on pulsewidth modulation (PWM) control and temperature inside the thermal chamber.

Let the error between the measured temperatures and model outputs at each time step k in vector form be

$$e(k,\theta) = [T_{c,e}(k,\theta)\ \ T_{s,e}(k,\theta)]^T - [T_{c,m}(k)\ \ T_{s,m}(k)]^T$$

where $\theta = [k_t\, c_p\, h]^T$, $T_{c,e}$, and $T_{s,e}$ represent the model parameters, core and surface temperatures, respectively. The battery is allowed to rest at ambient temperature to equilibrate, i.e., $x(0) = [T_\infty\ 0]^T$.

Parameters are identified by minimizing the Euclidean norm of the difference between the measured and simulated

TABLE II
IDENTIFIED THERMAL PROPERTIES

Parameter	Symbol	Value	Reference
Density	ρ	2047*	2118 [24]
Sp. heat coeff.	c_p	1109.2	1004.9–1102.6 [11], [25]
Thermal cond.	k_t	0.610	0.488–0.690 [9], [24]
Conv. coeff.	h	58.6	65.99 [25]

* Measured

temperatures as given by

$$\theta^* = \arg\min_{\theta} \sum_{k=1}^{N_f} ||e(k,\theta)||_2$$

where N_f is the number of measurement points. The minimization problem is solved using the *fmincon* function in MATLAB. The parameters in Table I are used as initial guess for the identification.

Table II shows the identified thermal properties for the 26650 battery. These parameters are close to the values reported in the literature. The identified specific heat coefficient c_p is 5% larger than the mean value determined in [11], where c_p was determined by measuring transient responses of the battery under different pulses. Forgez *et al.* suggested that the deviation in identified value of c_p might be caused by measurement uncertainty in temperature and the temperature dependency of the heat capacity. The identified thermal conductivity k_t is within the range of values presented in [9] and [24].

Despite using similar experimental data and setup, the identified convection coefficient is 11% smaller than the coefficient calculated by using thermal resistance and battery surface area in [25]. This difference between our identified value and the one in [25] may be due to the two different model structures. Lin *et al.* [25] considered two different materials, namely one for the core and one for the surface, whereas we assume the battery is a homogeneous and isotropic body. To accurately determine the convection coefficient, the temperature measurements of a pure metal during thermal relaxation can be used. For instance, the specific heat capacity of copper at 25 °C is known as 385 J/kgK. For more detailed description about the experiment, the interested reader is referred to [26].

Fig. 5 shows the measured and simulated temperatures at the core and surface of the battery. The error between the measurements and simulated temperature is less than the sensor accuracy of 0.5 °C. Thermocouples used for temperature measurements are T-type whose accuracy is the maximum of 0.5 °C or 0.4% according to technical information from the manufacturer, OMEGA. The parameterized thermal model accurately predicts the temperature inside the battery, which is difficult to measure in practical applications. Using (14), the temperature distribution inside the battery can be predicted, as shown in Fig. 6(a). Fig. 6(b) shows the volume-averaged temperature and its gradient of the battery, respectively. There is no significant difference between the volume-averaged temperature and the linear average of core and surface temperatures, i.e., $(T_s + T_c)/2$. It should be noted

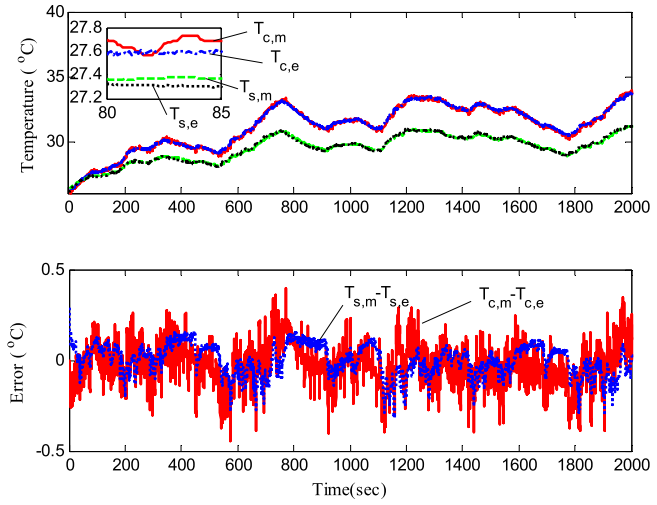

Fig. 5. Comparison between measured and simulated temperatures (top) and errors (bottom).

that existing approaches in [10], [11], and [13] have the capability of predicting the core temperature and have shown the efficacy of their proposed methods on the prediction of temperature inside the cell under consideration in this paper. However, the phenomena may differ in the case of a cell with larger radius [27]. The volume-averaged temperature gradient is different from the linear temperature gradient, i.e., $(T_s - T_c)/R$. In particular, the volume-averaged temperature gradient is 1.36 times greater than linear temperature gradient under the UAC test. Since nonuniform temperature distribution can lead to accelerated capacity losses of inner core [27], the volume-averaged temperature gradient is an important metric to describe severity of temperature inhomogeneity inside the battery.

B. Model Validation

To validate the performance of the reduced-order model with identified parameters, the battery was tested under a different HEV drive cycle, the escort convoy cycle (ECC) in [25]. The current and voltage profiles for this cycle are shown in Fig. 7(a). Fig. 7(b) shows that there are slight differences between the measured and simulated temperatures. In particular, the root-mean-square errors (RMSE) of core and surface temperatures are 0.4 °C and 0.3 °C, respectively. These differences may be explained with the assumption of radially uniform heat generation and high conductivity in the axial direction. Additionally, the entropy change of the LFP battery is not considered in heat generation formulation (17), which might introduce error in the calculation of heat generation rate. Furthermore, heat generation due to contact resistances between tabs and connecting wires can be another source of prediction error. At a high current rate, ohmic heating due to contact resistance could be substantially high. Nevertheless, since the comparison of temperatures shows a good agreement and reasonably small RMSEs, it can be concluded that the reduced-order model with identified thermal properties is reasonably accurate for thermal management during HEV drive cycles.

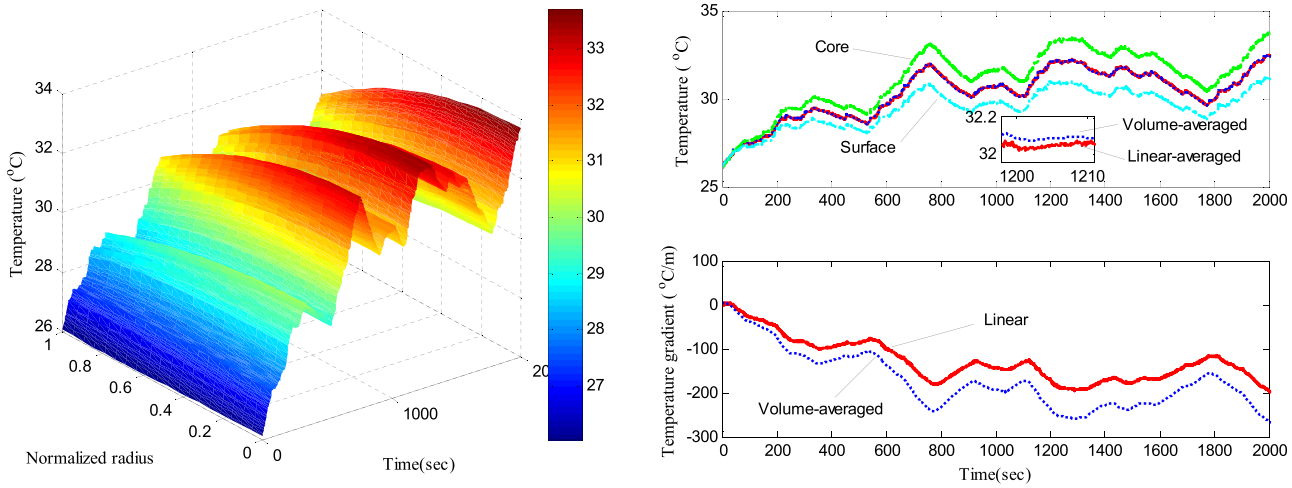

(a) (b)

Fig. 6. (a) Expected temperature distribution along the normalized radius (r/R) using PA. (b) Cell temperature (top) and temperature gradient (bottom).

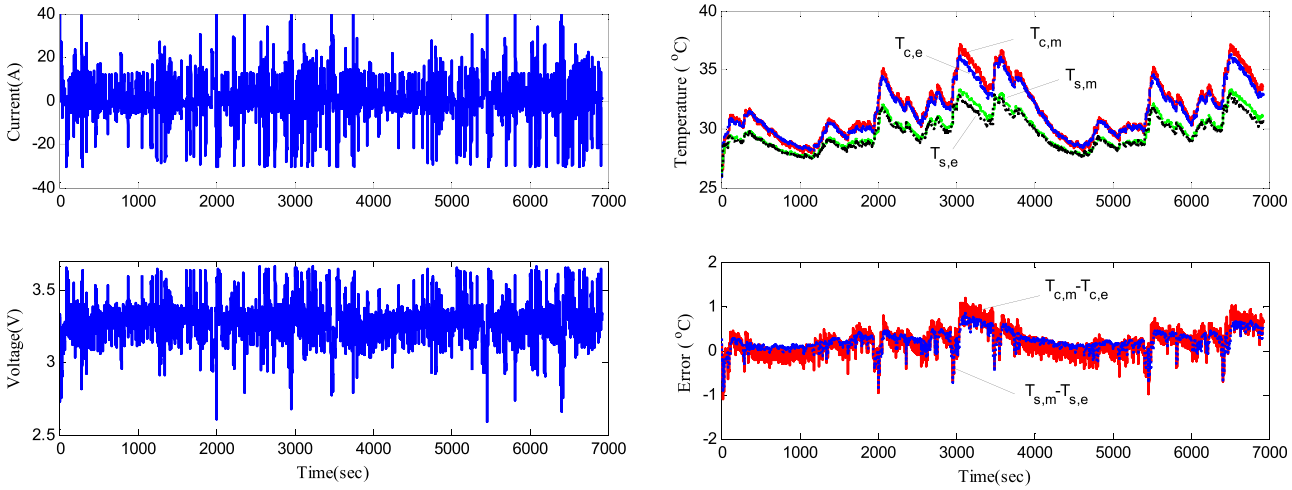

(a) (b)

Fig. 7. (a) Current (top) and voltage (bottom) profiles during ECC. (b) Validation data set: comparison between measured and simulated temperatures (top) and errors (bottom).

C. Parameter Sensitivity Analysis

Three parameters, the thermal conductivity k_t, the specific heat coefficient c_p and the convection coefficient h, are chosen for the sensitivity analysis. To investigate the impact of variations in parameters on the performance of temperature prediction, each parameter is varied between -20% and 20% around the identified value while holding the other parameters constant. Fig. 8 shows that the thermal conductivity and the specific heat coefficient have more influence on the prediction of the core temperature than the surface temperature. This result corresponds to the fact that the heat generated inside the battery is transferred through conduction. On the other hand, the prediction of the surface temperature is the most sensitive to the variation of the convection coefficient, which can be explained by the fact that the convection coefficient is directly related to the convective boundary condition (3). The convection coefficient has the most significant influence on the overall prediction of the core and the surface temperatures.

The specific heat coefficient and the thermal conductivity are weakly dependent on temperature [11], [28], [29], so the assumption of constant parameters can be justified. On the other hand, the convection coefficient depends strongly on fan speed or fluid velocity as expressed by empirical

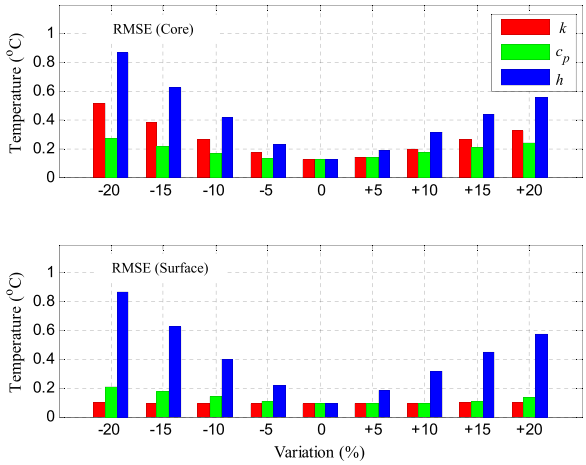

Fig. 8. Effect of parameter variation about the nominal values listed in Table II to temperature prediction: core (top) and surface (bottom).

correlations provided in [30]. Therefore, the accurate identification of the convection coefficient is important for better prediction of temperature inside the battery. This importance justifies the on-line identification of the convection coefficient for better estimation of temperature, as detailed in Section IV.

IV. Estimation of Temperature and Convection Coefficient

As discussed in Section III-C, the estimation of temperature inside the battery requires accurate knowledge of the convection coefficient, which depends on the cooling condition. To identify the convection coefficient and the core temperature inside the battery on-line, a DKF in [31] is applied. The other thermal parameters such as the thermal conductivity and the specific heat coefficient are constant values identified in Section III since these parameters have less influence on temperature and do not change significantly over time.

Assuming the input $u(t)$ is constant over each sampling interval Δt, a parameter varying discrete-time model at time step k can be obtained as

$$\begin{aligned} x_{k+1} &= \bar{A}(\theta_k)x_k + \bar{B}(\theta_k)u_k + w_k \\ y_k &= C(\theta_k)x_k + D(\theta_k)u_k + v_k \\ \theta_{k+1} &= \theta_k + r_k \end{aligned} \tag{18}$$

where $x = [\bar{T}\ \ \bar{\gamma}]^T$, $y = T_s$, $\theta = h$, and $u = [Q\ \ T_\infty]^T$. System matrices $\bar{A} \approx I + A\Delta t$ and $\bar{B} = B\Delta t$ are obtained from matrices in (16). Noise signals w_k, v_k, and r_k, are independent, zero-mean, Gaussian processes of covariance matrices Σ_w, Σ_v, and Σ_r, respectively.

The design of the DKF estimator is given as following update processes.

Time update for the parameter filter

$$\begin{aligned} \hat{\theta}_k^- &= \hat{\theta}_{k-1}^+ \\ S_k^- &= S_{k-1}^+ + \Sigma_r. \end{aligned}$$

Time update for the state filter

$$\begin{aligned} \hat{x}_k^- &= \bar{A}_{k-1}\hat{x}_{k-1}^+ + \bar{B}_{k-1}u_{k-1} \\ P_k^- &= \bar{A}_{k-1}P_{k-1}^+\bar{A}_{k-1}^T + \Sigma_w. \end{aligned}$$

Measurement update for the state filter

$$\begin{aligned} K_k &= P_k^- C_k^{xT}\left[C_k^x P_k^- C_k^{xT} + \Sigma_v\right]^{-1} \\ \hat{x}_k^+ &= \hat{x}_k^- + K_k\left[y_k - C(\hat{\theta}_k^-)\hat{x}_k^- - D(\hat{\theta}_k^-)u_k\right] \\ P_k^+ &= \left[I - K_k C_k^x\right]P_k^-. \end{aligned}$$

Measurement update for the parameter filter

$$\begin{aligned} L_k &= S_k^- C_k^{\theta T}\left[C_k^\theta P_k^- C_k^{\theta T} + \Sigma_e\right]^{-1} \\ \hat{\theta}_k^+ &= \hat{\theta}_k^- + L_k\left[y_k - C(\hat{\theta}_k^-)\hat{x}_k^- - D(\hat{\theta}_k^-)u_k\right] \\ S_k^+ &= \left[I - L_k C_k^\theta\right]S_k^- \end{aligned}$$

where superscripts $-$ and $+$ denote the *a priori* and *a posteriori* values, respectively. The matrices $\bar{A}_{k-1}$, C_k^x, and C_k^θ are calculated according to

$$\begin{aligned} \bar{A}_{k-1} &= \bar{A}(\theta_k)|_{\theta_k=\hat{\theta}_k^-} \\ C_k^x &= C(\theta_k)\Big|_{\theta_k=\hat{\theta}_k^-} \\ C_k^\theta &= \frac{dy_k}{d\theta_k}\Big|_{x_k=\hat{x}_k^-,\theta_k=\hat{\theta}_k^-}. \end{aligned}$$

The identified states $\hat{x}$ and parameter $\hat{\theta}$, computed from the above DKF algorithm, are used to estimate the core temperature in the battery from (15). It is noted that since the thermal system is linear, the DKF becomes a Kalman filter (KF) when the parameter of the convection coefficient is known or given. In other words, update processes for the parameter filter are unnecessary with the knowledge of convection coefficient.

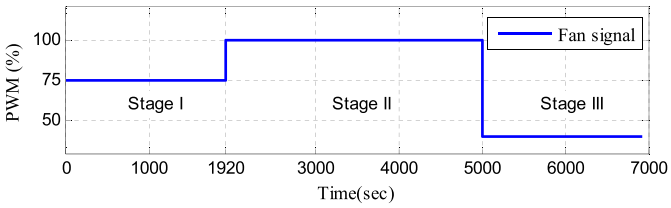

Fig. 9. Fan schedule for forced-air convective cooling.

V. Experimental Results

In this section, the performance of the proposed temperature estimator using the DKF is compared with that of the baseline KF estimator without parameter identification. Following the experimental setup in [25], we draw a current and measure voltage and temperatures at the core and the surface of the battery while controlling the ambient temperature in the thermal chamber. The surface temperature is used for the estimator and the core temperature is measured to verify the estimation accuracy. The experiment is performed using the ECC to verify the state and parameter estimation. Three different forced convective cooling conditions (stages I–III) are demonstrated using different PWM signals driving the fan, as shown in Fig. 9. To investigate the influence of change in the initial parameter on the temperature estimation, the parameter is provided to each estimator as following:

1) in stage I, the off-line predetermined convection coefficient is provided to the KF and is used for the DKF as an initial value: $\tilde{\theta} = \theta^*$ and $\hat{\theta}(0) = \theta^*$;
2) in stage II, the off-line predetermined convection coefficient is provided to the KF only: $\tilde{\theta} = \theta^*$;
3) in stage III, two times larger convection coefficient compared with the known value is provided to the KF: $\tilde{\theta} = 2\theta^*$

where $\tilde{\theta}$ and $\hat{\theta}$ denote fixed and identified parameters for the KF and the DKF, respectively, whereas θ^* presents the predetermined parameter value. Other thermal properties such as the thermal conductivity and the specific heat coefficient are assumed constant with values shown in Table I.

It is assumed that the initial temperature distribution inside the battery is uniform at 30 °C and convection coefficient

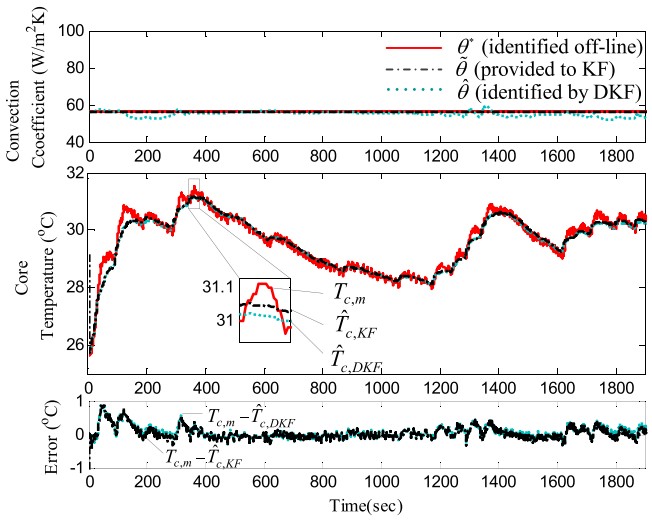

Fig. 10. Comparison of performance between KF estimator, DKF estimator during stage I: convection coefficient (top), core temperature (middle), and error (bottom).

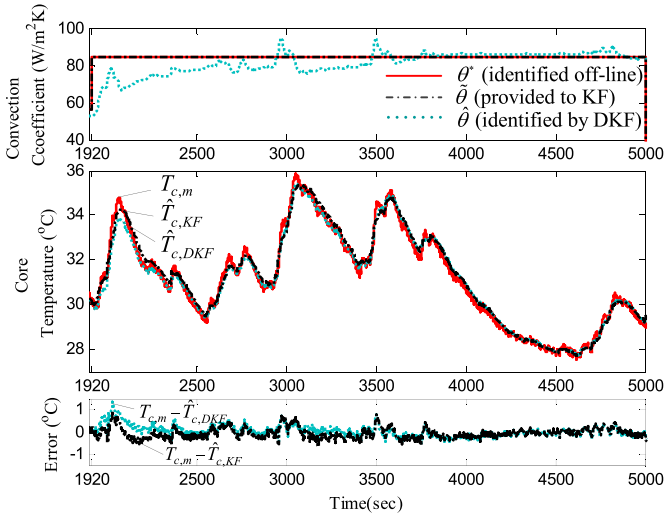

Fig. 11. Comparison of performance between KF estimator, DKF estimator during stage II: convection coefficient (top), core temperature (middle), and error (bottom).

is 56.2 W/m^{2}K, i.e., $\hat{x}(0) = [30\ 0]^T$ and $\hat{\theta}(0) = 56.2$, respectively. The covariance matrix for the state $\Sigma_w = {\beta_1}^2 \mathrm{diag}(1,1)$ describes the process noise, where $\beta_1 > 0$ is a parameter for tuning based on the model inaccuracy. The noise covariance $\Sigma_v = \sigma^2$ is determined from the standard deviation of temperature signal $\sigma = 0.05$ °C. The covariance matrix for the parameter $\Sigma_r = {\beta_2}^2$ influences the performance of noise filtering and the rate of parameter convergence. Ultimately, the initial condition of the error covariance matrix and the tuning parameter are chosen as $P(0) = \mathrm{diag}(1,1)$, $\beta_1 = 0.0005$, $S(0) = 0.05$, and $\beta_2 = 0.007$ through repeated simulations, respectively. It is noted that the initial conditions and tuning parameters for the DKF are the same as those of the KF.

The results for the parameter and state estimation are shown in Figs. 10–12 and summarized in Table III. Fig. 10 shows that all closed-loop estimators can accurately predict temperature inside the battery as evidenced by the small RMSE for

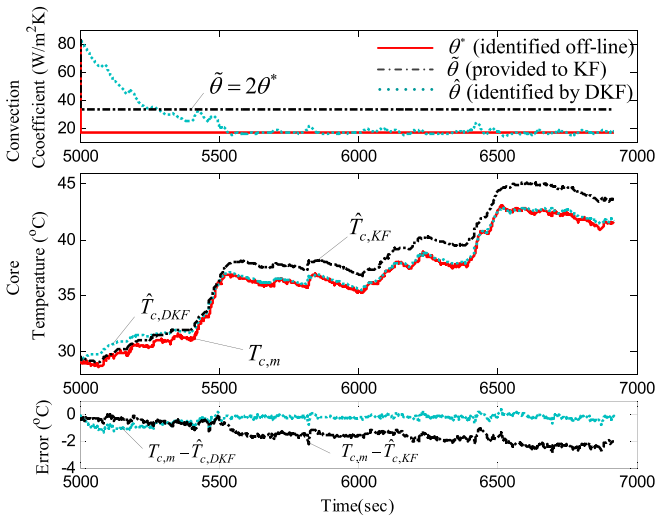

Fig. 12. Comparison of performance between KF estimator, DKF estimator during stage III: convection coefficient (top), core temperature (middle), and error (bottom).

TABLE III
PERFORMANCE OF CORE TEMPERATURE ESTIMATION: RMSEs

Method	Stage I	Stage II	Stage III
KF	0.18	0.24	1.58
DKF	0.18	0.25	0.45

temperature estimation, 0.18. On-line identified parameters are close to the off-line determined without large deviations during initial time periods, which is caused by two factors: 1) a correct initial guess for parameter and 2) a relatively small initial parameter covariance. Therefore, performances of the DKF estimator are comparable with that of KF estimator. As discussed in Section III-C, thermal properties can vary with respect to operating temperature. Therefore, it is expected that better performance can be achieved using temperature-dependent parameters for thermal conductivity and specific heat coefficient.

Fig. 11 shows the performance of temperature estimation by the closed estimator in stage II when there is a sudden change in the cooling condition. The KF can accurately estimate the core temperature with information about the change in the convection coefficient. Since the DKF is capable of identifying the convection coefficient online, the DKF provides reasonably accurate estimates for the core temperature by comparing the core temperature predicted by the KF estimator. The RMSE for core temperature estimation by the DKF is very close to the RMSE by the KF and this error is still reasonably small with considerations of the sensor accuracy.

As observed from Fig. 12, the KF estimator overestimates the core temperature when the incorrect parameter value is used as a convection coefficient. In other words, the reliable estimation of core temperature is only possible when the accurate parameter is available. Thus, it can be concluded that the DKF estimator outperforms the KF estimator due to the capability of parameter identification. The RMSE for core

temperature estimation in stage III can be substantially reduced from 1.58 to 0.45 by the DKF.

It is worth noting that the DKF can be augmented with other existing battery management strategies to improve the system robustness without cost increase. For instance, to detect partial blockage in a cooling system, typically, a mass flow or pressure sensor is required. The DKF enables the identification of the convection coefficient using sensors, which are already instrumented at the battery. The identified parameter can be also used for monitoring the malfunction or degradation of the cooling system. Under the assumption that the relationship between the convection coefficient and fan speed or PWM signal is known, the malfunction of the cooling system can be detected by comparing the identified parameter with the known value. When the difference between the identified and predetermined values $|\hat{\theta} - \theta^*|$ is bounded and small, it can be considered that there is no fault in the cooling system. On the other hand, $|\hat{\theta} - \theta^*| \gg \epsilon$, where ϵ is a pretuned threshold, a cooling fault can be detected. In particular, $|(\hat{\theta} - \theta^*)/\theta^*|$ can be interpreted as the severity of degradation of the cooling system.

VI. Conclusion

In this paper, a method to estimate the temperature distribution in cylindrical batteries under unknown cooling condition is proposed. First, a radially distributed 1-D thermal modeling approach for a cylindrical battery cell is considered. A PA is applied to obtain a reduced-order model enabling the development of real-time applications. Frequency domain analysis shows that the reduced-order model provides reasonably accurate prediction of the core and surface temperatures with an assumption that the temperature of cooling media does not change rapidly.

The reduced-order model is used to identify thermal properties such as the thermal conductivity and specific heat capacity of a 2.3 Ah 26650 LFP battery cell and the convection coefficient using a set of measured data: current, voltage, temperatures at the core and surface and ambient temperature. Identified parameters are close to the values reported in the literature. Particularly, the volume-averaged temperature gradient of a cylindrical cell captures the imbalance of temperature distribution, which is useful for battery management systems to minimize accelerated capacity losses of inner core. The numerical analysis on parameter sensitivity supports the use of constant parameters for thermal conductivity and heat capacity and the importance of identifying the convection coefficient on-line.

A DKF is applied to estimate the temperature inside the battery and convection coefficient by the cooling fan. The proposed method requires no knowledge of the convective cooling conditions. The results shows that the proposed DKF estimator can provide reasonably accurate estimates of core temperature and convection coefficient using surface temperature, which is relatively easy to measure in practice. In addition, a faulty operation in the cooling system can be detected by monitoring the difference between the identified and off-line predetermined values. Since forced air is used as a cooling media to reject heat from the cell in this paper, the range of the convection coefficient of which we are interested is less than 100 W/m^{2}K. Therefore, the reader is urged to investigate whether the PA is valid for their applications.

In the future, the proposed method can be used to develop various battery management strategies, e.g., the determination of maximum current with consideration of thermal constraints or optimal fan scheduling for energy efficiency, leading to the safe and efficient operation of the battery system.

References

[1] R. Huggins, *Advanced Batteries: Materials Science Aspects*, 1st ed. Berlin, Germany: Springer-Verlag, 2008.

[2] Z. Rao and S. Wang, "A review of power battery thermal energy management," *Renew. Sustain. Energy Rev.*, vol. 15, no. 9, pp. 4554–4571, 2011.

[3] J. Shim, R. Kostecki, T. Richardson, X. Song, and K. Striebel, "Electrochemical analysis for cycle performance and capacity fading of a lithium-ion battery cycled at elevated temperature," *J. Power Sour.*, vol. 112, no. 1, pp. 222–230, 2002.

[4] X. Zhang *et al.*, "Diagnostic characterization of high power lithium-ion batteries for use in hybrid electric vehicles," *J. Electrochem. Soc.*, vol. 148, no. 5, pp. 463–470, 2001.

[5] G. M. Ehrlich, "Lithium-ion batteries," in *Handbook of Batteries*, 3rd ed. New York, NY, USA: McGraw-Hill, 2002, ch. 35.

[6] S. Zhang, K. Xu, and T. Jow, "Low temperature performance of graphite electrode in li-ion cells," *Electrochim. Acta*, vol. 48, no. 3, pp. 241–246, 2002.

[7] Y. Kim, S. Mohan, J. B. Siegel, and A. G. Stefanopoulou, "Maximum power estimation of lithium-ion batteries accounting for thermal and electrical constraints," in *Proc. ASME Dyn. Syst. Control Conf.*, Palo Alto, CA, USA, Oct. 2013, pp. 11:35–11:55.

[8] Y. Kim, J. B. Siegel, and A. G. Stefanopoulou, "A computationally efficient thermal model of cylindrical battery cells for the estimation of radially distributed temperatures," in *Proc. Amer. Control Conf.*, Jun. 2013, pp. 698–703.

[9] M. Muratori, N. Ma, M. Canova, and Y. Guezennec, "A model order reduction method for the temperature estimation in a cylindrical li-ion battery cell," in *Proc. ASME Dyn. Syst. Control Conf.*, vol. 1. 2010, pp. 633–640.

[10] C. W. Park and A. K. Jaura, "Dynamic thermal model of li-ion battery for predictive behavior in hybrid and fuel cell vehicles," *SAE Trans., J. Engines*, vol. 112, no. 3, pp. 1835–1842, 2003.

[11] C. Forgez, D. Vinh Do, G. Friedrich, M. Morcrette, and C. Delacourt, "Thermal modeling of a cylindrical $LiFePO_4$/graphite lithium-ion battery," *J. Power Sour.*, vol. 195, no. 9, pp. 2961–2968, 2010.

[12] L. Cai and R. White, "An efficient electrochemical-thermal model for a lithium-ion cell by using the proper orthogonal decomposition method," *J. Electrochem. Soc.*, vol. 157, no. 11, pp. A1188–A1195, 2010.

[13] X. Lin, A. G. Stefanopoulou, H. E. Perez, J. B. Siegel, Y. Li, and R. D. Anderson, "Quadruple adaptive observer of the core temperature in cylindrical li-ion batteries and their health monitoring," in *Proc. Amer. Control Conf.*, Montreal, QC, Canada, Jun. 2012, pp. 578–583.

[14] Y. Kim, S. Mohan, J. B. Siegel, A. G. Stefanopoulou, and Y. Ding, "The estimation of radial temperature distribution in cylindrical battery cells under unknown cooling conditions," in *Proc. IEEE Conf. Decision Control*, Firenze, Italy, Dec. 2013, pp. 1–5.

[15] G. Plett, "High-performance battery-pack power estimation using a dynamic cell model," *IEEE Trans. Veh. Technol.*, vol. 53, no. 5, pp. 1586–1593, Sep. 2004.

[16] S. Al Hallaj, H. Maleki, J. Hong, and J. Selman, "Thermal modeling and design considerations of lithium-ion batteries," *J. Power Sour.*, vol. 83, nos. 1–2, pp. 1–8, 1999.

[17] D. R. Pendergast, E. P. DeMauro, M. Fletcher, E. Stimson, and J. C. Mollendorf, "A rechargeable lithium-ion battery module for underwater use," *J. Power Sour.*, vol. 196, no. 2, pp. 793–800, 2011.

[18] D. H. Jeon and S. M. Baek, "Thermal modeling of cylindrical lithium ion battery during discharge cycle," *Energy Convers. Manag.*, vol. 52, nos. 8–9, pp. 2973–2981, 2011.

[19] H. Maleki, S. A. Hallaj, J. R. Selman, R. B. Dinwiddie, and H. Wang, "Thermal properties of lithium-ion battery and components," *J. Electrochem. Soc.*, vol. 146, no. 3, pp. 947–954, 1999.

[20] S. Chen, C. Wan, and Y. Wang, "Thermal analysis of lithium-ion batteries," *J. Power Sour.*, vol. 140, no. 1, pp. 111–124, 2005.
[21] J. Shi, F. Wu, S. Chen, and C. Zhang, "Thermal analysis of rapid charging nickel/metal hydride batteries," *J. Power Sour.*, vol. 157, no. 1, pp. 592–599, 2006.
[22] D. Bernardi, E. Pawlikowski, and J. Newman, "General energy balance for battery systems," *J. Electrochem. Soc.*, vol. 132, no. 1, pp. 5–12, 1985.
[23] T.-K. Lee, Y. Kim, A. Stefanopoulou, and Z. Filipi, "Hybrid electric vehicle supervisory control design reflecting estimated lithium-ion battery electrochemical dynamics," in *Proc. Amer. Control Conf.*, 2011, pp. 388–395.
[24] H. Khasawneh *et al.*, "Analysis of heat-spreading thermal management solutions for lithium-ion batteries," in *Proc. ASME Conf.*, vol. 4. 2011, pp. 421–428.
[25] X. Lin *et al.*, "Online parameterization of lumped thermal dynamics in cylindrical lithium ion batteries for core temperature estimation and health monitoring," *IEEE Trans. Control Syst. Technol.*, vol. 21, no. 5, pp. 1745–1755, Sep. 2013.
[26] K. Onda, H. Kameyama, T. Hanamoto, and K. Ito, "Experimental study on heat generation behavior of small lithium-ion secondary batteries," *J. Electrochem. Soc.*, vol. 150, no. 3, pp. A285–A291, 2003.
[27] K. Smith, G.-H. Kim, and A. Pesaran, "Modeling of nonuniform degradation in large-format li-ion batteries," in *Proc. 215th Electrochem. Soc. Meeting*, San Francisco, CA, USA, May 2009, pp. 1–26.
[28] H. Maleki, J. Selman, R. Dinwiddie, and H. Wang, "High thermal conductivity negative electrode material for lithium-ion batteries," *J. Power Sour.*, vol. 94, no. 1, pp. 26–35, 2001.
[29] K. Onda, T. Ohshima, M. Nakayama, K. Fukuda, and T. Araki, "Thermal behavior of small lithium-ion battery during rapid charge and discharge cycles," *J. Power Sour.*, vol. 158, no. 1, pp. 535–542, 2006.
[30] A. Zukauskas, "Heat transfer from tubes in crossflow," in *Advances in Heat Transfer*, vol. 8, J. P. Hartnett and T. F. Irvine, Eds. Amsterdam, The Netherlands: Elsevier, 1972, pp. 93–160.
[31] E. A. Wan and A. T. Nelson, *Dual Extended Kalman Filter Methods*. New York, NY, USA: Wiley, 2002, pp. 123–173.

Youngki Kim (M'14) received the B.S. and M.S. degrees from the School of Mechanical and Aerospace Engineering, Seoul National University, Seoul, Korea, and the Ph.D. degree in mechanical engineering from the University of Michigan, Ann Arbor, MI, USA, in 2001, 2003, and 2014, respectively.

He was a Research Engineer with the Research and Development Division, Hyundai Motor Company, Seoul, from 2003 to 2008. His current research interests include the modeling and estimation of electrochemical energy storage systems, and control of hybrid powertrain systems. He is currently a Post-Doctoral Research Fellow with the Powertrain Control Laboratory, University of Michigan.

Shankar Mohan (S'11) received the bachelor's degree in electrical engineering from the National University of Singapore, Singapore, and the master's degree in electrical engineering from the University of Michigan, Ann Arbor, MI, USA, in 2011 and 2013, respectively, where he is currently pursuing the Ph.D. degree in electrical engineering.

His current research interests include numerical optimization methods and the application of control techniques to energy systems.

Jason B. Siegel (M'08) received the B.S., M.S., and Ph.D. degrees in electrical engineering from the University of Michigan, Ann Arbor, MI, USA, in 2004, 2006, and 2010, respectively.

He is currently an Assistant Research Scientist with the Mechanical Engineering Department, University of Michigan. He is currently being involved in developing techniques to measure *in situ* the lithium concentration gradients inside an operational battery using neutron imaging for the validation of electrochemical models. His current research interests include modeling, model validation, and control of electrochemical energy conversion and storage systems.

Anna G. Stefanopoulou (F'09) is a Professor of mechanical engineering and the Director with the Automotive Research Center, University of Michigan, Ann Arbor, MI, USA. From 1996 to 1997, she was a Technical Specialist with Ford Motor Company, Dearborn, MI, USA. From 1998 to 2000, she was an Assistant Professor with the University of California, Santa Barbara, CA, USA. She has authored and co-authored more than 200 papers and a book on estimation and control of internal combustion engines and electrochemical processes, such as fuel cells and batteries. She holds nine U.S. patents.

Prof. Stefanopoulou is a fellow of the American Society of Mechanical Engineers. She was a recipient of four Best Paper Awards.

Yi Ding is currently a Senior Research Engineer with Ground Vehicle Power and Mobility, U.S. Army Tank Automotive Research, Development, and Engineering Center, Warren, MI, USA. He is involved in conducting energy storage research and development status, and assisting the Energy Storage Team in monitoring technical progress of Research and Development projects. He has more than 20 years of experience in battery research and development, and project management.